Cell, Vol. 95, 927–937, December 23, 1998, Copyright ©1998 by Cell Press

# The Structural Basis of Estrogen Receptor/Coactivator Recognition and the Antagonism of This Interaction by Tamoxifen

**Andrew K. Shiau,* Danielle Barstad,† Paula M. Loria,† Lin Cheng,† Peter J. Kushner,‡ David A. Agard,*§ and Geoffrey L. Greene†§**
*Howard Hughes Medical Institute
and the Department of Biochemistry and Biophysics
University of California at San Francisco
San Francisco, California 94143-0448
†The Ben May Institute for Cancer Research
and Department of Biochemistry and Molecular Biology
University of Chicago
Chicago, Illinois 60637
‡Metabolic Research Unit
University of California
San Francisco, California 94143

## Summary

**Ligand-dependent activation of transcription by nuclear receptors (NRs) is mediated by interactions with coactivators. Receptor agonists promote coactivator binding, and antagonists block coactivator binding. Here we report the crystal structure of the human estrogen receptor α (hERα) ligand-binding domain (LBD) bound to both the agonist diethylstilbestrol (DES) and a peptide derived from the NR box II region of the coactivator GRIP1 and the crystal structure of the hERα LBD bound to the selective antagonist 4-hydroxytamoxifen (OHT). In the DES-LBD-peptide complex, the peptide binds as a short α helix to a hydrophobic groove on the surface of the LBD. In the OHT-LBD complex, helix 12 occludes the coactivator recognition groove by mimicking the interactions of the NR box peptide with the LBD. These structures reveal the two distinct mechanisms by which structural features of OHT promote this "autoinhibitory" helix 12 conformation.**

## Introduction

Estrogens exert their physiological effects by binding to the estrogen receptors, which are members of the nuclear receptor (NR) superfamily of ligand-inducible transcription factors (Tsai and O'Malley, 1994; Beato et al., 1995). The estrogen receptor α (ERα) regulates the differentiation and maintenance of neural, skeletal, cardiovascular, and reproductive tissues (Korach, 1994; Smith et al., 1994). Compounds that modulate ERα transcriptional activity are currently being used to treat osteoporosis, cardiovascular disease, and breast cancer (Gradishar and Jordan, 1997; Jordan, 1998).

All ERα ligands bind exclusively to the C-terminal ligand-binding domain (LBD). The LBD recognizes a variety of compounds diverse in their size, shape, and chemical properties. Some of these ligands, including the endogenous estrogen 17β-estradiol ($E_2$) and the synthetic nonsteroidal estrogen diethylstilbestrol (DES), function as pure agonists, whereas others, such as ICI-164,384, function as pure antagonists. Synthetic ligands such as tamoxifen and raloxifene (RAL) belong to a growing class of molecules known as selective estrogen receptor modulators (SERMs), which function as antagonists in specific tissue and promoter contexts (Grese et al., 1997). The remarkable tissue-specific behavior of tamoxifen was recently demonstrated in the National Surgical Adjuvant Breast and Bowel Project–sponsored Breast Cancer Prevention Trial (Smigel, 1998). In the group of women at high risk for breast cancer who received tamoxifen treatment, there was an increased incidence of endometrial cancer but a reduced occurrence of certain bone fractures and a dramatic 45% reduction in breast cancer incidence. The rational design of new SERMs and the optimization of existing ones require an understanding of the effects of different ligand chemistries and structures upon ERα transcriptional activity.

Transcriptional activation by ERα is mediated by at least two separate activation functions (AFs), AF-1 in the N terminus, and AF-2 in the LBD. The activity of AF-1 is regulated by growth factors acting through the MAP kinase pathway (Kato et al., 1995), while AF-2 activity is responsive to ligand binding (Kumar et al., 1987). The binding of agonists triggers AF-2 activity, whereas the binding of antagonists does not (Berry et al., 1990).

Recent structural studies suggest that ligands regulate AF-2 activity by directly affecting the structure of the LBD. Comparison of the structure of the unliganded human retinoid X receptor α LBD (Bourguet et al., 1995) with the structures of the agonist-bound LBDs of the human retinoic acid receptor γ (RARγ) (Renaud et al., 1995) and other NRs suggests that an agonist-induced conformational change involving the repositioning of helix 12, the most C-terminal helix of the LBD, is essential for AF-2 activity (Moras and Gronemeyer, 1998). Because certain point mutations in helices 3, 5, and 12 abolish AF-2 activity but have no effect on ligand or DNA binding, these regions of the LBD have been predicted to form part of a recognition surface, created in the presence of agonist, for molecules that link the receptor to the general transcriptional machinery (Danielian et al., 1992; Wrenn and Katzenellenbogen, 1993; Henttu et al., 1997; Feng et al., 1998).

The structures of the LBD complexed with $E_2$ and RAL show that, although both ligands bind at the same site within the core of the LBD (Brzozowski et al., 1997), each of these ligands induces a different conformation of helix 12. Whereas helix 12 in the $E_2$-LBD complex packs against helices 3, 5/6, and 11 in a conformation that has been observed for the corresponding helix in other agonist-bound NR LBD structures, helix 12 in the RAL-LBD complex is bound in a hydrophobic groove composed of residues from helices 3 and 5. This alternative orientation of helix 12 partially buries residues in the groove that are necessary for AF-2 activity, suggesting that RAL and possibly other antagonists block AF-2 function by disrupting the topography of the AF-2 surface.

§To whom correspondence should be addressed (e-mail: agard@msg.ucsf.edu or ggreene@huggins.bsd.uchicago.edu).

Several proteins, including SRC-1/N-CoA1 (Onate et al., 1995; Kamei et al., 1996), GRIP1/TIF2/N-CoA2 (Hong et al., 1996; Voegel et al., 1996; Torchia et al., 1997;), p/CIP/RAC3/ACTR/AIB1 (Anzick et al., 1997; Chen et al., 1997; Li et al., 1997; Torchia et al., 1997), and CBP/p300 (Hanstein et al., 1996), associate in a ligand-dependent manner with the ERα. These proteins have been classified as transcriptional coactivators because they enhance ligand-dependent transcriptional activation by the ERα as well as by several other NRs (Horwitz et al., 1996; Glass et al., 1997). SRC-1 and GRIP1 bind to the agonist-bound LBDs of both the human thyroid receptor β (TRβ) and human ERα using the putative AF-2 interaction surface (Feng et al., 1998). Members of the p160 family of coactivators, such as SRC-1 and GRIP1, as well as other coactivators, recognize agonist-bound NR LBDs through a short signature sequence motif, LXXLL (where L is leucine and X is any amino acid), known as the NR box (Le Douarin et al., 1996; Heery et al., 1997; Torchia et al., 1997; Ding et al., 1998). Mutagenesis studies indicate that the affinity of coactivators for NR LBDs is determined principally, if not exclusively, by these NR boxes (Le Douarin et al., 1996; Heery et al., 1997; Torchia et al., 1997; Ding et al., 1998).

The structural mechanisms by which binding of different ligands to ERα influences coactivator recruitment remain unclear. We have chosen to examine the structural and functional effects on the LBD of the binding of two chemically related compounds, the agonist, DES, and the selective antagonist, 4-hydroxytamoxifen (OHT), the active metabolite of tamoxifen (Grainger and Metcalfe, 1996). Here we report the 2 Å resolution structure of the ERα LBD bound to both DES and a peptide with the sequence of the second NR box (NR box II) from the p160 coactivator GRIP1, and the 1.9 Å X-ray crystal structure of the human ERα LBD bound to OHT. In the DES complex, the NR box peptide is bound in an α-helical conformation by a hydrophobic groove formed by residues from helices 3, 4, 5, and 12 and the turn between helices 3 and 4. In the OHT complex, rather than forming part of a functional AF-2 surface, helix 12 binds to and occludes the coactivator recognition site by mimicking the interactions formed by an NR box with the LBD. The two distinct mechanisms by which specific structural features of OHT direct this alternative conformation of helix 12 are discussed.

## Results

### Structure Determination

GRIP1, a mouse p160 coactivator, interacts both in vivo and in vitro with the ERα LBD bound to agonist (Ding et al., 1998), but not with the LBD bound to antagonist (Norris et al., 1998). Mutational studies of GRIP1 and its human homolog TIF2 suggest that of the three NR boxes from GRIP1, NR box II (residues 690 to 694) binds most tightly to the ERα LBD (Ding et al., 1998; Voegel et al., 1998). Competition assays indicate that a 13-residue peptide, $NH_2$-KHKILHRLLQDSS-$CO_2H$ (residues 686 to 698 from GRIP1), containing NR box II, binds specifically to the agonist-bound ERα LBD ($IC_{50} < 0.4$ μM; P. J. K., unpublished) and to other agonist-bound NR LBDs (Darimont et al., 1998 [see Note Added in Proof]; Ding et al., 1998). In the present study, an electrophoretic mobility shift assay was used to demonstrate that the NR box II peptide bound the ERα LBD in the presence of the agonist DES but not the antagonist OHT (data not shown). In combination, these observations suggest that the NR box II peptide is a valid model for studying the interaction between GRIP1 and the ERα LBD.

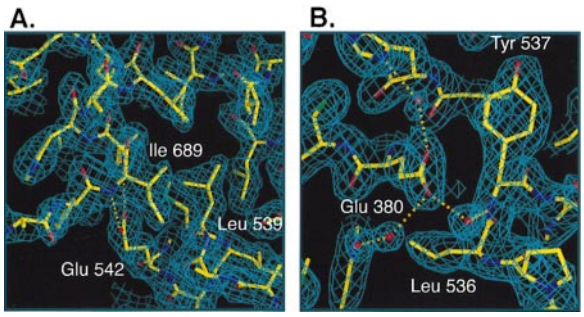


Figure 1. Views of the Electron Density of the DES-ERα LBD-GRIP1 NR Box II Peptide Complex and of the OHT-ERα LBD Complex

(A) A view of a $2F_o-F_c$ electron density map of the DES-LBD-peptide complex calculated at 2.03 Å resolution and contoured at 1.0 σ showing the GRIP1 NR box II interaction with the LBD. The peptide was omitted from the model prior to map calculation. Ile-689 from the peptide and two of the three receptor residues with which it interacts (Glu-542 and Leu-539) are labeled. Asp-538 has been omitted for clarity. The hydrogen bonds between the γ-carboxylate of Glu-542 and the amides of residues 689 and 690 of the peptide are depicted as dashed orange bonds.

(B) A view of a $2F_o-F_c$ electron density map of the OHT-LBD complex calculated at 1.90 Å resolution and contoured at 1.0 σ showing the N-terminal region of helix 12. The dashed orange bonds depict the water-mediated hydrogen bond network between the imidazole ring of His-377, the γ-carboxylate of Glu-380, and the amide of Tyr-537. The three labeled residues (Glu-380, Leu-536, and Tyr-537) interact with each other through van der Waals contacts and/or hydrogen bonds.

In order to characterize structurally the interaction between the GRIP1 NR box II peptide and the ERα LBD, recombinant human ERα LBD (residues 297–554) was crystallized bound to both DES and the peptide. The ERα LBD bound to OHT was also crystallized in order to determine the mechanism by which this antagonist blocks coactivator/ERα interaction. X-ray diffraction data from these crystals were measured, and the structures were determined by a combination of molecular replacement (using a modified version of the coordinates of the RARγ LBD [Renaud et al., 1995] as the search model) and aggressive density modification (see Experimental Procedures). The structure of the DES-ERα LBD-NR-box II peptide complex has been refined to a crystallographic R factor of 19.9% ($R_{free}$ = 25.0%) using data to 2.03 Å resolution (Figure 1A and Table 1). The structure of the OHT-ERα LBD complex has been refined using data to 1.90 Å to a crystallographic R factor of 23.0% ($R_{free}$ = 26.2%) (Figure 1B and Table 1).

### Overall Structure of the DES-LBD-NR Box II Peptide Complex

The asymmetric unit of the DES-LBD-NR box II peptide complex crystals contains the same noncrystallographic dimer of LBDs that has been observed in the previously

Table 1. Summary of Crystallographic Statistics

| Data Collection | | |
|---|---|---|
| Ligand | DES | OHT |
| Space group | $P2_1$ | $P6_522$ |
| Resolution | 2.03 | 1.90 |
| Observations | 104,189 | 269,253 |
| Unique | 30,265 | 23,064 |
| Completeness (%) | 98.4 | 99.1 |
| $R_{sym}$ (%)[a] | 7.8 | 7.0 |
| Average I/σI | 9.8 | 16.1 |
| **Refinement** | | |
| No. of nonhydrogen atoms | 4,180 | 2,069 |
| $R_{cryst}$ (%)[b]/$R_{free}$ (%) | 19.9/25.0 | 23.0/26.2 |
| Bond rms deviation (Å) | 0.005 | 0.006 |
| Angle rms deviation (°) | 1.05 | 1.04 |
| Average B factor (Å$^2$) | 34.0 | 40.4 |

[a] $R_{sym} = \Sigma_i|I_i - \langle I_i\rangle|/\Sigma_i I_i$, where $\langle I_i\rangle$ is the average intensity over symmetry equivalents.
[b] $R_{cryst} = \Sigma|F_o - F_c|/\Sigma|F_o|$.

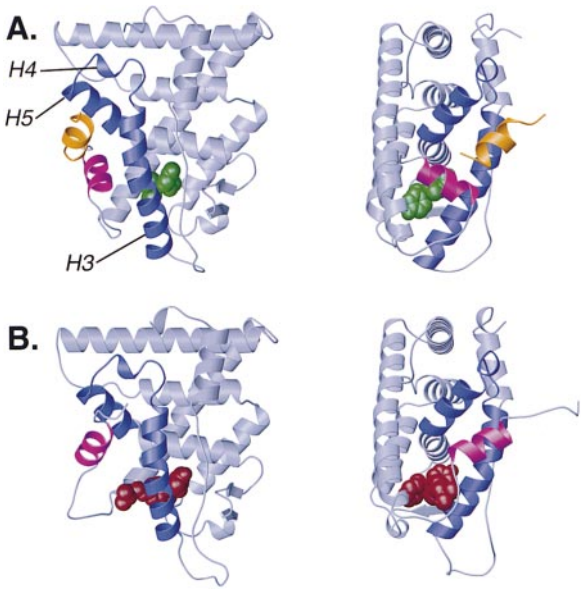


Figure 2. Overall Structures of the DES-ERα LBD-GRIP1 NR Box II Peptide Complex and of the OHT-ERα LBD Complex

(A) Two orthogonal views of the DES-ERα LBD-NR box II peptide complex. The coactivator peptide and the LBD are shown as ribbon drawings. The peptide is colored gold, and helix 12 (residues 538–546) is colored magenta. Helices 3, 4, and 5 (labeled H3, H4, and H5, respectively) are colored blue. DES, colored green, is shown in space-filling representation.

(B) Two orthogonal views of the OHT-ERα LBD complex similar to those of the agonist complex in (A). The LBD is depicted as a ribbon drawing. As in (A), helix 12 (residues 536–544) is colored in magenta, and helices 3, 4, and 5 are colored blue. OHT, in red, is shown in space-filling representation.

determined structures of the LBD bound to both $E_2$ and RAL (Brzozowski et al., 1997; Tanenbaum et al., 1998). The conformation of each LBD complexed with DES closely resembles that of the LBD bound to $E_2$ (Brzozowski et al., 1997); each monomer is a wedge-shaped molecule consisting of three layers of 11 to 12 helices and a single beta hairpin (Figure 2A). One NR box II peptide is bound to each LBD in a hydrophobic cleft composed of residues from helices 3, 4, 5, and 12 and the turn between 3 and 4 (Figures 2A and 3A). The density for both peptides in the asymmetric unit is continuous and unambiguous (Figure 1A). Residues 687 to 697 from peptide A and residues 686 to 696 from peptide B have been modeled; the remaining residues are disordered. Given that each peptide lies within a different environment within the crystal, it is striking that from residues Ile-689 to Gln-695 each peptide forms a two-turn, amphipathic α helix (Figures 2A and 3A). Flanking this region of common secondary structure, the peptides adopt dissimilar random coil conformations.

### The NR Box II Peptide-LBD Interface

The binding of the NR box II peptide to the ERα LBD buries 1000 Å$^2$ of predominantly hydrophobic surface area from both molecules. The NR box II peptide-binding site is a shallow groove composed of residues Leu-354, Val-355, Ile-358, Ala-361, and Lys-362 from helix 3; Phe-367 and Val-368 from helix 4; Leu-372 from the turn between helices 3 and 4; Gln-375, Val-376, Leu-379, and Glu-380 from helix 5; and Asp-538, Leu-539, Glu-542, and Met-543 from helix 12 (Figure 3A). The floor and sides of this groove are completely nonpolar, but the ends of this groove are charged (Figure 3C).

The LBD interacts primarily with the hydrophobic face of the NR box II peptide α helix formed by the side chains of Ile-689 and the three LXXLL motif leucines (Leu-690, Leu-693, and Leu-694). The side chain of Leu-690 is deeply embedded within the groove and forms van der Waals contacts with the side chains of Ile-358, Val-376, Leu-379, Glu-380, and Met-543 (Figures 3A and 3C). The side chain of Leu-694 is similarly isolated within the groove and makes van der Waals contacts with the side chains of Ile-358, Lys-362, Leu-372, Gln-375, Val-376, and Leu-379 (Figures 3A and 3C). In contrast, the side chains of both Ile-689 and the second NR box leucine, Leu-693, rest against the rim of the groove (Figures 3A and 3C). The side chain of Ile-689 lies in a shallow depression formed by the side chains of Asp-538, Leu-539, and Glu-542. The side chain of Leu-693 makes nonpolar contacts with the side chains of Ile-358 and Leu-539.

In addition to interacting with the hydrophobic face of the peptide helix, the LBD stabilizes the main chain conformation of the NR box peptide by forming capping interactions with both ends of the peptide helix. Glu-542 and Lys-362 are positioned at opposite ends of the peptide-binding site (Figure 3A). The γ-carboxylate of Glu-542 hydrogen bonds to the amides of the residues of N-terminal turn of the peptide helix (residues 688 and 689 of peptide A; residues 689 and 690 of peptide B) (Figure 1A). Similarly, the ε-amino group of Lys-362 hydrogen bonds to the carbonyls of the residues of the C-terminal turn of the peptide helix (residue 693 of peptide A; residues 693 and 694 of peptide B) (Figure 5). The side chain of Gln-375 also forms a water-mediated hydrogen bond to the carbonyl of residue 694.

To test the importance of the NR box peptide/LBD interface observed in the crystal, a series of site-directed mutations were introduced into the LBD. These mutations were designed either to perturb the nonpolar character of the floor of the binding groove (Ile-358→Arg,

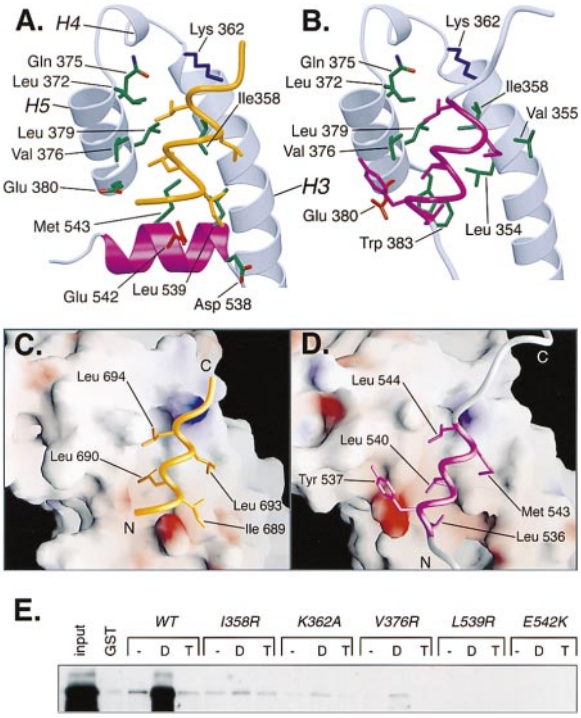


Figure 3. The NR Box II Peptide/DES-LBD Interface and the Helix 12/OHT-LBD Interface

(A) A close-up view of the coactivator peptide bound to the DES-LBD complex. The regions of the LBD that do not interact with the peptide have been omitted for clarity. Helices 3, 4, and 5 are labeled H3, H4, and H5, respectively. The side chains of the receptor residues that interact with the peptide are depicted. Except for Lys-362 (blue) and Glu-542 (red), the side chains are colored by atom type (carbon and sulfur atoms are colored green, oxygen atoms are colored red, and nitrogen atoms are colored blue). Helix 12 is colored magenta. The peptide, colored gold, is depicted as a Cα worm; only the side chains of Ile-689 and the three motif leucines (Leu-690, Leu-693, and Leu-694) are drawn.

(B) A close-up view of the OHT-LBD complex showing helix 12 bound to part of the coactivator-binding site. Only the side chains of residues that interact with helix 12 are drawn (with the exception of the side chain of His-373, which is omitted for clarity). Except for Lys-362 (blue) and Glu-380 (red), the side chains are colored by atom type (as specified in [A]). Residues 530–551 are depicted as a Cα worm; residues 536–544 are colored magenta. The side chains of Leu-536, Tyr-537, Leu-540, Met-543, and Leu-544 are shown.

(C) A molecular surface representation of the LBD bound to DES colored according to the local electrostatic potential (blue = positive; red = negative) as calculated in GRASP (Nicholls et al., 1991). The coactivator peptide is depicted as in (A) and the view is equivalent to that in (A). The side chains of Leu-690 and Leu-694 are bound in a hydrophobic groove, and those of Ile-689 and Leu-693 rest against the edge of this groove.

(D) A molecular surface representation of the LBD bound to OHT colored as in (C). Residues 530–551 are depicted as in (B) and the view is equivalent to that in (B). Whereas the side chains of Leu-540 and Leu-544 are embedded in the hydrophobic groove, that of Met-543 lies along the edge of this groove.

(E) $^{35}$S-labeled GRIP1 was incubated with either immobilized glutathione S-transferase (GST), immobilized wild-type GST-hERα LBD (WT), or immobilized mutant GST-LBDs in the absence of ligand (−) or in the presence of DES (D) or OHT (T). Thirty picomoles of each of the GST-LBDs were immobilized, as described in the Experimental Procedures. The bound GRIP1 was visualized by fluorography after SDS-PAGE. The input lane represents the total amount of $^{35}$S-GRIP1 included in each binding reaction. All of the mutations in the LBD disrupt agonist-dependent binding of GRIP1.

Val-376→Arg, and Leu-539→Arg) or to prevent the formation of the capping interactions (Lys-362→Ala and Glu-542→Lys) (Feng et al., 1998). Fusions of glutathione S-transferase (GST) to the wild-type and mutant LBDs were analyzed for their ability to bind $^{35}$S-labeled GRIP1 in the absence of ligand or in the presence of DES or OHT. Only the wild-type GST-LBD was able to recognize the coactivator in the presence of DES (Figure 3E), confirming the importance of the observed capping and hydrophobic packing interactions.

### Agonist Recognition

In its receptor complex, DES, like $E_2$ (Brzozowski et al., 1997), is completely encased within the narrower half of the LBD in a predominantly hydrophobic cavity composed of residues from helices 3, 6, 7, 8, 11, and 12 as well as the S1/S2 hairpin (Figures 2A and 4A).

The interaction of DES with ERα resembles that of $E_2$. One of the phenolic rings of DES lies in the same position as the $E_2$ A ring near helices 3 and 6. Like the aromatic ring of the $E_2$, the DES A ring (Figure 4A) is engaged by the side chains of Phe-404, Ala-350, Leu-387, and Leu-391 with its phenolic hydroxyl forming hydrogen bonds to the γ-carboxylate of Glu-353, to the guanidinium group of Arg-394, and to a structurally conserved water molecule. The A′ ring of DES (Figure 4A) is bound near helices 7, 8, and 11 adjacent to the location of the $E_2$ C and D rings. This ring forms van der Waals contacts not only with Gly-521 and Leu-525, like the D ring of $E_2$, but also with Met-343, Leu-346, and Met-421 (Figure 4A). Even though it is located 1.7 Å from the position of the D ring hydroxyl, the DES A′ ring phenolic hydroxyl is still able to hydrogen bond to the imidazole ring of His-524 (Figure 4A).

DES also forms contacts with the LBD that $E_2$ does not. There are unoccupied cavities adjacent to the α face of the B ring and the β face of the C ring of the $E_2$ (Brzozowski et al., 1997; Tanenbaum et al., 1998). The ethyl groups of DES, which project perpendicularly from the plane of the phenolic rings, fit snugly into these spaces. The resulting additional nonpolar contacts with the side chains of Ala-350, Leu-384, Phe-404, and Leu-428 (Figure 4A) may account for the higher affinity of DES for the receptor (Kuiper et al., 1997).

Except for Met-421 and Met-528 (both of which contact only DES) and Met-388 and Ile-424 (both of which contact only $E_2$), the ER is able to use the same residues to form all of the observed hydrogen bonds and van der Waals contacts with both of these distinctly shaped agonists (Figure 4A and Brzozowski et al., 1997; Tanenbaum et al., 1998). This remarkable adaptability is presumably the result of both the relatively large molecular volume of the binding pocket (∼500 Å$^3$ in both complexes) and its apparent structural plasticity. In particular, at the DES A′ ring/steroid D ring end of the binding pocket, Met-343, Met-421, His-524, and Met-528 adopt different packing configurations in response to each ligand (data not shown).

### Structure of the OHT-LBD Complex

The binding of OHT induces a conformation of the LBD that differs in both secondary and tertiary structural organization from that driven by DES binding. In the DES

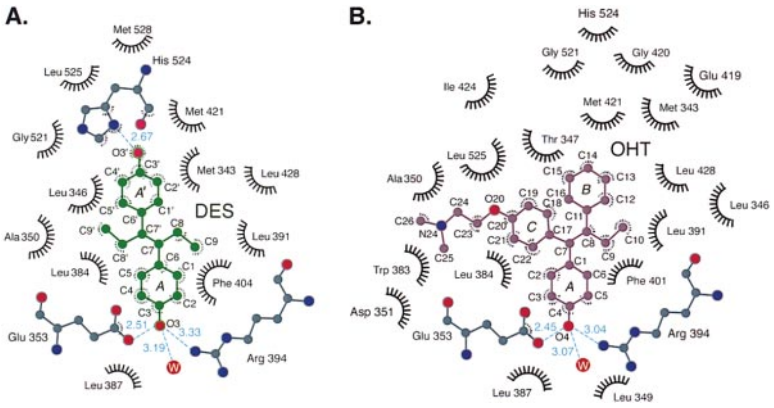


Figure 4. DES Interactions with the LBD (A) and OHT Interactions with the LBD (B)

Residues that interact with the ligands are drawn at approximately their true positions. The residues that form van der Waals contacts with ligand are depicted as labeled arcs with radial spokes that point towards the ligand atoms with which they interact. The residues that hydrogen bond to ligand are shown in ball-and-stick representation. Hydrogen bonds are represented as dashed cyan lines; the distance of each bond is given. The ligand rings and the individual ligand atoms are labeled.

complex, the main chain from residues 339 to 341, 421 to 423, and 527 to 530 forms parts of helices 3, 8, and 11, respectively. In contrast, these regions adopt an extended conformation in the OHT complex (Figures 2A, 2B, and 6A). In addition, the composition and orientation of helix 12 are different in the two structures. Helix 12 in the DES complex consists of residues 538 to 546, whereas helix 12 in the OHT complex consists of residues 536 to 544. Most dramatically, rather than covering the ligand-binding pocket as it does in the DES complex, helix 12 in the OHT complex occupies the part of the coactivator-binding groove formed by residues from helices 3, 4, and 5 and the turn connecting helices 3 and 4 (Figures 2A, 2B, and 3B). This alternative conformation of helix 12 appears to be similar to that observed in the RAL complex (Brzozowski et al., 1997).

### Helix 12–LBD Interface

Except for the orientation of helix 12, the structure of the peptide-binding groove is almost identical in the DES-LBD-NR box II peptide, OHT-LBD, and $E_2$-LBD complexes (Figures 3A and 3B) (Brzozowski et al., 1997). We therefore refer to the region of this groove outside of helix 12 as the "static region" of the NR box–binding site (Feng et al., 1998). Helix 12 in the OHT complex and the NR box peptide helix in the DES complex interact with the static region of the coactivator recognition groove in strikingly similar ways.

Helix 12 mimics the hydrophobic interactions of the NR box peptide with the static region of the groove with a stretch of residues (residues 540 to 544) that resembles an NR box (LLEML instead of LXXLL). The side chains of Leu-540 and Met-543 lie in approximately the same locations as those of the first and second motif leucines (Leu-690 and Leu-693) in the peptide complex (Figure 5). Leu-540 is inserted into the groove and makes van der Waals contacts with Leu-354, Val-376, and Glu-380 (Figures 3B and 3D). Met-543 lies along the edge of the groove and forms van der Waals contacts with the side chains of Leu-354, Val-355, and Ile-358 (Figures 3B and 3D). The side chain position of Leu-544 almost exactly overlaps that of the third NR box leucine, Leu-694 (Figure 5). Deep within the groove, the Leu-544 side chain makes van der Waals contacts with the side chains of Ile-358, Lys-362, Leu-372, Gln-375, Val-376, and Leu-379 (Figures 3B and 3D).

Helix 12 in the OHT complex is also stabilized by N- and C-terminal capping interactions. Lys-362 interacts with the C-terminal turn of helix 12 much as it does with the equivalent turn of the peptide helix (Figures 3A and 3B). The Lys-362 side chain packs against the C-terminal turn of helix 12 with its ε-amino group hydrogen bonding to the carbonyls of residues 543 and 544 (Figure 5). Given that the capping interaction at the N-terminal turn of the coactivator helix is formed by a helix 12 residue (Glu-542), the N-terminal turn of helix 12 in the antagonist complex is stabilized by another residue, Glu-380 (Figures 3B and 3D). The Glu-380 γ-carboxylate forms van der Waals contacts with Tyr-537 and interacts with the amide of Tyr-537 through a series of water-mediated hydrogen bonds (Figure 1B).

In addition to forming these "NR box–like" interactions, helix 12 also forms van der Waals contacts with areas of the LBD outside of the coactivator recognition groove. The side chain of Leu-536 forms van der Waals contacts with Glu-380 and Trp-383, and that of Tyr-537 forms van der Waals contacts with His-373, Val-376,

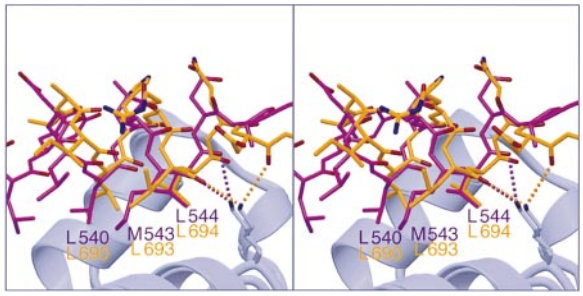


Figure 5. Comparison of Helix 12 from the OHT Complex and the NR Box II Peptide

The structures of the OHT-LBD complex and the DES-LBD-NR box II peptide complex were overlapped using the Cα coordinates of residues 306–526 of the LBD. Helix 12 from the DES-LBD-coactivator peptide complex is omitted for clarity. Residues 536–551 (helix 12 = residues 536–544) from the OHT-LBD complex are colored magenta, and the peptide is colored gold. For the OHT-LBD complex, the hydrogen bonds between the ε-amino group of Lys-362 and the backbone carbonyls of residues 543 and 544 of helix 12 are illustrated as dashed magenta bonds. For the DES-LBD-peptide complex, the hydrogen bonds between the ε-amino group of Lys-362 and the backbone carbonyls of residues 693 and 696 of the coactivator peptide are depicted as dashed orange bonds. Helix 12: L540 = Leu-540; M543 = Met-543; L544 = Leu-544. Peptide: L690 = Leu-690; L693 = Leu-693; L694 = Leu-694.

and Glu-380 (Figures 1B, 3B, and 3D). As a result of these contacts, helix 12 in the OHT complex buries more solvent-accessible surface area (~1200 Å$^2$) than the NR box peptide in the DES complex.

### OHT Recognition

OHT is bound within the same pocket that recognizes DES, $E_2$, and RAL. The orientation of OHT within the binding pocket appears to be dictated by the positioning of two structural features of this ligand, the phenolic A ring and the bulky side chain (Figures 4B and 6C). The A ring of OHT is bound in approximately the same location as the A ring of DES near helices 3 and 6, with its phenolic hydroxyl hydrogen bonding to a structurally conserved water and to the side chains of Glu-353 and Arg-394 (Figure 4B). Like the bulky side chain of RAL, the side chain of OHT exits the binding pocket between helices 3 and 11 (Figures 2B and 4B). The OHT C ring (Figure 4B) forms van der Waals contacts with the side chains of Met-343, Leu-346, Thr-347, Ala-350, Trp-383, Leu-384, Leu-387, and Leu-525. The positioning of the flexible dimethylaminoethyl region of the side chain is stabilized by van der Waals contacts with Thr-347, Ala-350, and Trp-383 and by a salt bridge between the dimethylamino group of the side chain and the β-carboxylate of Asp-351, which lies 3.8 Å away (Figure 4B). The positions of the A ring and the side chain in the context of the rigid triphenylethylene framework of OHT requires that the ethylene group of OHT lie in an orientation nearly orthogonal to that of the ethylene group of DES (Figures 4A, 4B, and 6D). As a result, the B ring of OHT is driven more deeply into the binding pocket than the A′ ring of DES (Figures 6B and 6C).

This location of the OHT B ring apparently cannot be accommodated by the same mechanisms that allow the DES A′ ring/$E_2$ D ring end of the binding pocket to adapt to the different structural features of DES and $E_2$. Instead, the residues that contact the B ring (Met-343, Leu-346, Met-421, Ile-424, Gly-521, His-524, and Leu-525), most of which also interact with the A′ ring of DES, adopt conformations distinct from the ones they adopt in the DES structure (Figure 6D). In fact, the location of the B ring actually precludes the side chain of one residue, Met-421, from adopting the same conformation that it adopts in the DES structure (Figures 6B and 6C). As a consequence of these B ring–induced side chain conformations, many interresidue van der Waals contacts present in the DES complex are absent in the OHT complex. For example, whereas Met-421 packs against His-524 from helix 11 and against Met-343 from helix 3 in the agonist complexes, it is precluded by the location of the OHT B ring from interacting with either of these residues in the antagonist complex (Figure 6D).

The structural effects of the placement of the B ring are not limited to the residues that contact the B ring; the conformations of these residues force other residues throughout the binding pocket to, in turn, adopt alternative conformations. For instance, the conformation of Met-421 in the OHT complex prevents the side chains of Phe-404 and Phe-425 from occupying the positions they take in the DES complex (Figures 6B and 6C). The alternative conformations of the side chains of both the residues that directly contact the B ring and those that are indirectly affected by it force the main chain throughout the binding pocket to adopt a different conformation as well (Figure 6D).

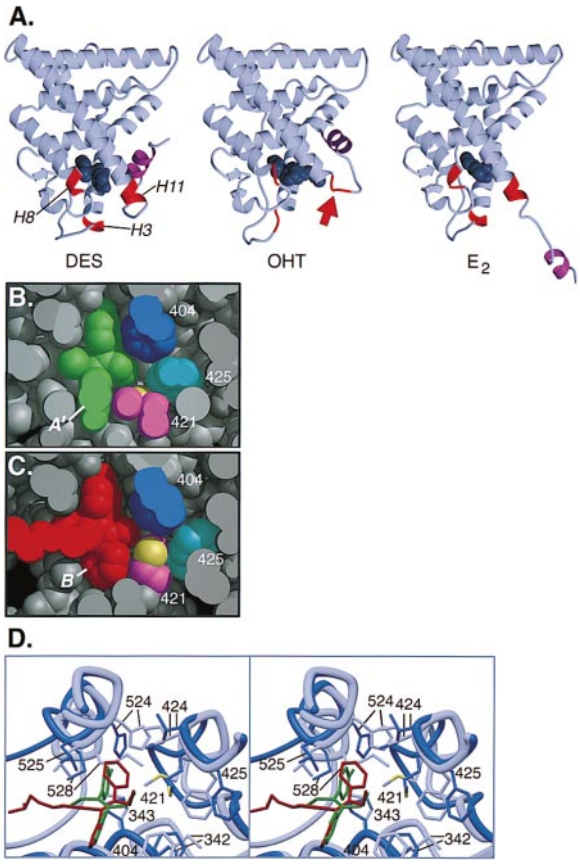


Figure 6. The Binding of Agonists and Antagonists Promote Different LBD Conformations

(A) Ribbon representations of the DES complex (without the coactivator peptide), the OHT complex, and the $E_2$ complex of Tanenbaum et al. (1998). The hormones are shown in space-filling representation. In each complex, helix 12 is colored magenta, and the main chain of residues 339 to 341, 421 to 423, and 527 to 530 is colored red. Helices 3, 8, and 11 (H3, H8, and H11, respectively) are labeled in the DES complex.

(B) A cross section of a space-filling model of the LBD bound to DES (green) showing the ligand completely embedded in the ligand-binding cavity. The A′ ring of DES (A′), Phe-404 (404), Met-421 (421), and Phe-425 (425) are labeled. The carbon atoms of side chain of Met-421 are colored magenta, and the sulfur atom is colored yellow.

(C) A cross section of a space-filling model of the LBD bound to OHT (red). The view is equivalent to that in (B). The B rings of OHT (B), Phe-404 (404), Met-421 (421), and Phe-425 (425) are labeled. The side chain of Met-421 is colored as in (B). The conformation of the B ring forces Met-421 to adopt a different conformation than the one it adopts in the DES complex (compare with [B]).

(D) The structures of the OHT complex and the DES complex were overlapped as in Figure 5. OHT is colored red, and DES is colored green. The A rings of both ligands point out of the page; the B ring of OHT and the A′ ring of DES point into the page. The LBD bound to OHT is colored blue, and the LBD bound to DES is colored light gray. The side chains of some of the residues whose conformations are dramatically different between the two complexes are drawn: Met-342 (342); Met-343 (343); Phe-404 (404); Met-421 (421); Ile-424 (424); Phe-425 (425); His-524 (524); Leu-525 (525); Met-528 (528). The sulfur atom of Met-421 is colored yellow in both structures.

## Discussion

### The AF-2 Surface and NR Box Recognition

The structure of the ERα LBD in complex with the GRIP1 NR box II peptide reveals that the LXXLL motif forms the core of a short amphipathic α helix that is recognized by a highly complementary groove on the surface of the receptor. In agreement with the conclusions of other mutational and structural studies (Brzozowski et al., 1997; Feng et al., 1998), we propose that this peptide-binding groove formed by residues from helices 3, 4, 5, and 12 and the turn between helices 3 and 4 is the AF-2 surface of ERα.

Of the eleven AF-2 residues whose side chains interact with the coactivator helix (Figure 3A), only four (Lys-362, Leu-379, Gln-375, and Glu-542) are highly conserved across the nuclear receptor family (Wurtz et al., 1996). The side chains of Gln-375 and Leu-379 are predominantly buried even in the absence of GRIP1 binding and appear to form integral parts of the architecture of the AF-2 surface. In contrast, the side chains of Lys-362 and Glu-542 are largely solvent exposed in the absence of coactivator and make both nonpolar contacts and the only direct receptor-mediated polar interactions with the coactivator helix. These two capping interaction residues are perfectly positioned at opposite ends of the AF-2 surface groove not only to stabilize the main chain conformation of the coactivator but also to function as a molecular caliper; the 15 Å distance between Lys-362 and Glu-542 is well suited to measure off the ~11 Å axial length of the short, two-turn coactivator α helix (Figure 3C). Similar receptor-mediated capping interactions have also been observed in a complex between the TRβ LBD and the NR box II peptide (Darimont et al., 1998). Mutation of either of these two capping interaction residues severely cripples coactivator binding by ERα as well as by TRβ (see Results and Henttu et al., 1997; Feng et al., 1998). Hence, the formation of helix-capping interactions may be a general feature of coactivator recognition by NRs.

The hydrophobic face of the NR box helix is formed by the side chains of the three motif leucines and the isoleucine preceding the motif (Ile-689). The functional importance of the conserved leucines in receptor binding has been demonstrated by numerous studies (Le Douarin et al., 1996; Heery et al., 1997; Torchia et al., 1997; Ding et al., 1998; Voegel et al., 1998). Structural and biochemical data in this study implicate Ile-689 as another key ERα-binding determinant. In the crystal, only the side chains of the motif leucines and Ile-689 extensively contact the LBD in both noncrystallographic symmetry-related peptides. Mutation of Ile-689 to alanine reduces the ability of the NR box II peptide to inhibit the binding of GRIP1 to ERα by ~30-fold in a competition assay (data not shown). Remarkably, the residue preceding the LXXLL motif differs for the three NR boxes of GRIP1/TIF2. The sequence variability at this position may explain the apparently different affinities of the NR boxes of TIF2 for the ERα (Voegel et al., 1998).

### Helix 12 and the Regulation of AF-2 Activity

ERα AF-2 activity is blocked by antagonists such as OHT and RAL. The most striking feature of the structures of the OHT- and RAL-liganded ERα LBDs is that helix 12 is bound to the static region of the coactivator recognition groove (Figure 3B and Brzozowski et al., 1997). A comparison of these two structures with the structure of the coactivator/LBD complex reveals that in the antagonist complexes, the region of helix 12 with an NR box–like sequence (LXXML versus LXXLL) functions as an intramolecular mimic of the coactivator helix (Figure 5 and Brzozowski et al., 1997). Consistent with the proposals of others (Brzozowski et al., 1997; Darimont et al., 1998), this disposition of helix 12 directly affects the structure and function of the AF-2 surface in two ways. First, because helix 12 residues form an integral part of the AF-2 surface, the AF-2 surface is incomplete when helix 12 is in the antagonist-bound conformation. In particular, Leu-539, Glu-542, and Met-543 are incorrectly oriented for coactivator recognition. Second, residues from the static region of the AF-2 surface are bound to helix 12 and are prevented from interacting with coactivator (Figures 3A and 3B).

The sequence similarity of helix 12 of the ERα LBD to the LXXLL motif is not shared by all other NRs; the identities of the residues in this region of helix 12 in most NRs, although generally hydrophobic in character, do not as closely resemble the sequence of an NR box as those of ERα (Wurtz et al., 1996). However, it is possible that an intramolecular inhibitor with a suboptimal recognition sequence would compete for coactivator binding given its extremely high local concentration. Therefore, it will be necessary to determine if the antagonists of other NRs act by the same mechanism.

### The Structural Basis of OHT Antagonism

The binding of OHT to ERα promotes a helix 12 conformation that inhibits binding of coactivator. OHT does not directly interact with any helix 12 residues (Figure 4B). Moreover, the structure of the LBD in the region of the AF-2 surface groove that interacts with helix 12 in the OHT complex is the same in the DES and $E_2$ complexes (Figures 3A, 3B, and 5) (Brzozowski et al., 1997). So how does OHT binding influence the position of helix 12?

Numerous studies have demonstrated the importance of the OHT side chain in receptor antagonism (Jordan and Gosden, 1982; Robertson et al., 1982). A comparison of the structures of the OHT and DES complexes reveals that the binding mode of the OHT side chain precludes the agonist-induced conformation of helix 12. The OHT side chain projects out of the ligand-binding pocket between helices 3 and 11 (Figures 2B, 6B, and 6C). As a result, the positioning of helix 12 over the ligand-binding pocket, as it is in the agonist-bound conformation, would bury the positively charged dimethylamino group of the OHT side chain within a hydrophobic cavity and produce steric clashes between the dimethylaminoethyl region of side chain and the side chain of Leu-540.

In functional terms, OHT is not, however, simply "an agonist with a side chain." OHT binding promotes a conformation of the LBD that is distinct from that stabilized by either DES or $E_2$ binding. These different conformations impose different restrictions on the positioning of helix 12.

Helices 3, 8, and 11 in the DES and $E_2$ complexes are between one to two turns longer than they are in the OHT complex (Figure 6A and Brzozowski et al., 1997). Helix 11 ends at Cys-530 in the DES and $E_2$ complexes and at Tyr-526 in the OHT complex. Helix 12 begins at Leu-536 in the OHT complex. This appears to be necessary; in the antagonist complex, Leu-536 forms a cooperative network of nonpolar contacts and hydrogen bonds with Glu-380 and Tyr-537 that stabilizes the N terminus of helix 12 (Figure 1B). Therefore, if helix 12 were to bind the static region of the AF-2 surface in the presence of agonist, the loop connecting helices 11 and 12 would be required to span ~17 Å over five residues. Although theoretically possible, this conformation would be highly strained and hence unlikely. In contrast, the longer loop connecting helices 11 and 12 in the OHT complex allows helix 12 to extend to the static region of the coactivator-binding groove.

In the DES and $E_2$ complexes, helix 12 and the loop connecting helices 11 and 12 pack against helices 3 and 11, whereas they do not in the OHT complex (Figures 2A and 2B and Brzozowski et al., 1997). Are the longer helices in the DES and $E_2$ complexes dependent upon the interactions helix 12 forms in the agonist-bound conformation? A recently described structure of the $E_2$-LBD complex suggests that they are not (Tanenbaum et al., 1998). In this structure, a crystal-packing artifact forces helix 12 to contact a symmetry-related molecule. Helix 12 is clearly not positioned over the ligand-binding pocket in this structure. Nevertheless, helices 3, 8, and 11 are longer than they are in the OHT complex (Figure 6A). Hence, the longer helices of the agonist complexes occur independently of the positioning of helix 12 over the ligand-binding pocket and are instead a direct result of agonist binding.

The secondary structure differences between the agonist complexes and the OHT complex arise from distinct arrangements of packing interactions induced by the different ligands. A cooperative network of van der Waals contacts, organized around DES or $E_2$, between various hydrophobic residues from helices 3, 7, 8, and 11 and the β hairpin appears to stabilize the longer helices in the agonist complexes (Figures 4A and 6D). The placement of the OHT B ring forces many of the ligand-binding pocket residues that surround it to adopt conformations that are dramatically different from those they adopt in either the DES or $E_2$ structures (see Results). As a result, many of the interresidue packing interactions present in the DES and $E_2$ structures are either absent or altered in the OHT structure (Figure 6D). These structural distortions apparently force the main chain from residues 339 to 341, 421 to 423, and 527 to 530 (which form parts of helices 3, 8, and 11, respectively, in the agonist structures) to adopt an extended conformation in the OHT structure (Figures 6A–6D).

Therefore, the binding of OHT has two distinct effects on the positioning of helix 12, each of which contributes to antagonism. Helix 12 is prevented from being positioned over the ligand-binding pocket by the OHT side chain. In addition, the alternative packing arrangement of ligand-binding pocket residues around OHT stabilizes a conformation of the LBD that permits helix 12 to reach the static region of the AF-2 surface and mimic bound coactivator.

These mechanisms do not appear to be specific to OHT. The side chain of RAL, like that of OHT, sterically hinders the agonist-bound conformation of helix 12 (Brzozowski et al., 1997). In addition, helix 11 appears to end at Met-528 in the RAL complex. This may result from the distortions in the binding pocket in the vicinity of His-524 directed by RAL binding (Brzozowski et al., 1997).

There is a great need for the improvement of existing therapies and the development of new ones for the prevention and treatment of breast cancer. While the tissue-selective antagonism of SERMs such as OHT and RAL is the result of numerous factors (Grainger and Metcalfe, 1996; Grese et al., 1997; Jordan, 1998), dissection of the mechanisms of action of these ligands requires a comprehensive understanding of how they act on the LBD and regulate its interactions with other cellular factors. Our studies have revealed, unexpectedly, that ligand-mediated structural perturbations in and around the ligand-binding pocket, and not simply side chain effects, contribute to receptor antagonism. Adjusting the balance between these two effects provides a novel strategy for the design of improved SERMs.

## Experimental Procedures

### Protein Expression and Purification

Human ERα LBD (residues 297–554) was expressed in BL21(DE3)-pLysS (harboring a plasmid provided by P. Sigler) as described previously (Seielstad et al., 1995). Bacterial lysates were applied to an estradiol-Sepharose column (Greene et al., 1980), and bound hERα LBD was carboxymethylated with 5 mM iodoacetic acid (Hegy et al., 1996). Protein was eluted with $3 \times 10^{-5}$ M ligand in 30–100 ml of 50 mM Tris, 1 mM EDTA, 1 mM DTT, and 250 mM NaSCN (pH 8.5). The hERα LBD was further purified by ion exchange chromatography (Resource Q, Pharmacia). Protein samples were analyzed by SDS-PAGE, native PAGE, and electrospray ionization mass spectrometry.

### GST-Pulldown Assays

A fusion between GST and amino acids 282–595 of hERα was constructed by subcloning the EcoRI fragment from pSG5 ERα-LBD (Lopez et al., submitted) into pGEX-3X (Pharmacia). Mutations were introduced into this construct using the QuikChange Kit (Stratagene) or by subcloning the appropriate fragments of mutant derivatives of pSG5-ER-HEGO (Tora et al., 1989; Feng et al., 1998). All constructs were verified by automated sequencing.

The wild-type and mutant GST-LBDs were expressed in BL21(DE3) cells. The total [$^3$H]$E_2$ binding activity in each extract was determined by saturation analysis using a controlled pore glass bead (CPG) assay (Greene et al., 1988). GST-LBD protein levels were also monitored by Western blotting with a monoclonal antibody to hERα (H222) to confirm that the mutant GST-LBDs bound $E_2$ with affinities comparable to the wild-type protein. Cleared extracts containing the GST-LBDs were incubated in buffer alone (50 mM Tris [pH 7.4], 150 mM NaCl, 2 mM EDTA, 1 mM DTT, 0.5% NP-40, and a protease inhibitor cocktail) or with 1 μM of either DES or OHT for 1 hr at 4°C. Extract aliquots containing 30 pmol of binding activity, based on the CPG assay, were then incubated with 10 μl glutathione-Sepharose-4B beads (Pharmacia) for 1 hr at 4°C. Beads were washed five times with 20 mM HEPES (pH 7.4), 400 mM NaCl, and 0.05% NP-40. $^{35}$S-labeled GRIP1 was synthesized using the TNT Coupled Reticulocyte Lysate System (Promega) and pSG5-GRIP1 (a gift of M. Stallcup) as the template. Immobilized GST-LBDs were incubated for 2.5 hr with 2.5 μl aliquots of crude translation reaction mixture diluted in 300 μl of Tris-buffered saline (TBS). After five washes in TBS containing 0.05% NP-40, proteins were eluted by boiling the beads for 10 min in sample buffer. Bound $^{35}$S-GRIP1 was visualized by fluorography following SDS-PAGE.

**Crystallization and Data Collection**

Crystals of the DES-hERα LBD-GRIP1 NR box II peptide complex were obtained by hanging drop vapor diffusion at 19°C–21°C. Prior to crystallization, the DES-LBD complex was incubated with a 2- to 4-fold molar excess of the GRIP1 NR box II peptide for 7–16 hr. Samples (2 μl) of this solution (4.3 mg/ml protein) were mixed with 2 μl of the reservoir buffer consisting of 25%–27% (w/v) PEG 4000, 90 mM Tris (pH 8.75–9.0), and 180 mM Na acetate and suspended over wells of the reservoir buffer. These crystals lie in the space group $P2_1$ with cell parameters a = 54.09 Å, b = 82.22 Å, c = 58.04 Å, and β = 111.34. Two molecules of the DES-LBD complex and of the coactivator peptide form the asymmetric unit. A crystal was transferred to a cryosolvent solution containing 25% (w/v) PEG 4000, 10% (w/v) ethylene glycol, 100 mM Tris (pH 8.5), 200 mM Na acetate, and 10 μM peptide and frozen in an $N_2$ stream at −170°C in a rayon loop. Diffraction data were measured at −170°C using the 300 mm MAR image plate at the Stanford Synchrotron Radiation Laboratory (SSRL) beamline 7-1 (λ = 1.08 Å).

Crystals of the OHT-hERα LBD complex were obtained by hanging drop vapor diffusion at 21°C–23°C. Samples (2 μl) of a solution containing 3.9 mg/ml complex and 2 μl of the reservoir solution containing 9% (w/v) PEG 8000, 6% (w/v) ethylene glycol, 50 mM HEPES (pH 6.7), and 200 mM NaCl were mixed and suspended over wells of the reservoir solution. These crystals lie in the space group $P6_522$ with cell parameters a = b = 58.24 Å and c = 277.47 Å. The asymmetric unit consists of a single LBD monomer; the dimer axis lies along a crystallographic 2-fold. A crystal was briefly incubated in a cryoprotectant solution consisting of 10% (w/v) PEG 8000, 25% (w/v) ethylene glycol, 50 mM HEPES (pH 7.0), and 200 mM NaCl and then flash frozen in liquid $N_2$ suspended in a rayon loop. Diffraction data were measured at −170°C at SSRL beamline 9-1 (λ = 0.98 Å) using a 345 MAR image plate.

The images of both data sets were processed with DENZO (Otwinowski and Minor, 1997), and both data sets were scaled with SCALEPACK (Otwinowski and Minor, 1997) using the default −3σ cutoff.

**Structure Determination and Refinement**

Our initial efforts to determine the structure of the DES-LBD-peptide complex utilized a low resolution (3.1 Å) data set (data not shown). The two LBDs in the asymmetric unit were located by molecular replacement in AMoRe (CCP4, 1994) using a partial polyalanine model of the human retinoic acid receptor γ LBD (Renaud et al., 1995) as the search probe (R= 58.2%, CC= 35.6% after placement of both monomers). Iterative cycles of 2-fold NCS averaging in DM (CCP4, 1994) interspersed with model building in MOLOC (Muller et al., 1988) and model refinement in REFMAC (Murshudov et al., 1997) (using tight NCS restraints and phases from 2-fold averaging) were used to quickly build a model of the LBD alone. For this procedure, MAMA (Kleywegt and Jones, 1994) was used for all mask manipulations, and PHASES (Furey and Swaminathan, 1990) and the CCP4 suite (CCP4, 1994) were used for the generation of structure factors and the calculation of weights.

At this point, although the DES-LBD complex model accounted for ~90% of the scattering matter in the asymmetric unit, refinement was being hampered by severe model bias. The OHT complex data set was then collected (Table 1). Starting with one of the monomers of the preliminary DES-LBD model as the search probe, molecular replacement in AMoRe was used to search for the location of LBD in this crystal form in both $P6_122$ and $P6_522$. A translation search in $P6_522$ yielded the correct solution (R= 53.8%, CC = 38.2%). In order to reduce model bias, DMMULTI (CCP4, 1994) was then used to project averaged density from the DES complex cell into the OHT complex cell. Using MOLOC, a model of the LBD was built into the resulting density. The model was refined initially in REFMAC and later with the simulated annealing, positional, and B-factor refinement protocols in X-PLOR (Brünger, 1996) using a maximum-likelihood target (Adams et al., 1997). Anisotropic scaling and a bulk solvent correction were used, and all B-factors were refined isotropically. Except for the $R_{free}$ set (a random sampling consisting of 8% of the data set), all data between 41 and 1.9 Å (with no σ cutoff) were included. The final model consists of residues 306–551, the ligand, and 79 waters. According to PROCHECK (CCP4, 1994), 91.6% of all residues in the model are in the core regions of the Ramachandran plot and none are in the disallowed regions.

The high resolution data set of the DES-LBD NR box II peptide complex (Table 1) became available when the $R_{free}$ of the OHT-LBD model was ~31%. Both monomers in the asymmetric unit of the DES complex crystal were relocated using AMoRe and the incompletely refined OHT-LBD model (with helix 12 and the loop between helices 11 and 12 removed) as the search model. The missing parts of the model were built, and the rest of the model was corrected using MOLOC and 2-fold averaged maps generated in DM. Initially, refinement was carried out with REFMAC, using tight NCS restraints. At later stages, the model was refined without NCS restraints using the simulated annealing, positional, and B-factor refinement protocols in X-PLOR and a maximum-likelihood target. All B-factors were refined isotropically, and anisotropic scaling and a bulk solvent correction were used. The $R_{free}$ set contains a random sample of 6.5% of all data. In refinement, all data between 27 and 2.03 Å (with no σ cutoff) were used. The final model is composed of residues 305–549 of monomer A, residues 305–461 and 470–549 of monomer B, residues 687–697 of peptide A, residues 686–696 of peptide B, two ligand molecules, 147 waters, two carboxymethyl groups, and a chloride ion. According to PROCHECK, 93.7% of all residues in the model are in the core regions of the Ramachandran plot, and none are in the disallowed regions.

**Illustrations**

Figures 3C and 3D were created using GRASP (Nicholls et al., 1991). Figures 1, 2, 3A, 3B, 5, 6A, and 6D were generated using BOBSCRIPT (Esnouf, 1997) and rendered using Raster3D (Merritt and Anderson, 1994). Figure 4 was generated using LIGPLOT (Wallace et al., 1995), and Figures 6B and 6C were created using MidasPlus (Huang et al., 1991). Figure 1A depicts peptide B; all other illustrations of the coactivator peptide depict peptide A.

**Acknowledgments**

This work has been supported by funds from the U.S. Army Medical and Research Material Command grant DAMD 17-94-J-4228 (G. L. G.), the NCI Cancer Center Support grant P30 CA-14599 (G. L. G.), the Howard Hughes Medical Institute (D. A. A.), the NIGMS grant GM31627 (D. A. A.), the American Cancer Society grant BE61 (P. J. K.), and the NIH grant DK51083 (P. J. K.). A. K. S. was supported by a Howard Hughes Medical Institute Predoctoral Fellowship and a UCSF Chancellor's Fellowship. The Stanford Synchrotron Radiation Laboratory (SSRL) is funded by the Department of Energy, Office of Basic Energy Science. We thank H. Deacon, P. Foster, T. Mau, N. Sauter, and the staff of SSRL for assistance with data collection; C. Anderson, C. Hospelhorn, and T. McSherry for assistance with the biochemical experiments; and M. Butte, B. Darimont, R. Keenan, T. Mau, R. Wagner, and K. Yamamoto for comments on the manuscript. We would especially like to thank R. Wagner for contributions at the early stages of the project; D. Tanenbaum, Y. Wang, and P. Sigler for providing us their $E_2$-LBD coordinates in advance of publication; and H. Deacon and A. Derman for cheerful and extensive assistance with the figures and the manuscript, respectively.

Received September 1, 1998; revised November 16, 1998.

**References**

Adams, P.D., Pannu, N.S., Read, R.J., and Brünger, A.T. (1997). Cross-validated maximum likelihood enhances crystallographic simulated annealing refinement. Proc. Natl. Acad. Sci. USA *94*, 5018–5023.

Anzick, S.L., Kononen, J., Walker, R.L., Azorsa, D.O., Tanner, M.M., Guan, X.-Y., Sauter, G., Kallioniemi, O.-P., Trent, J.M., and Meltzer, P.S. (1997). AIB1, a steroid receptor coactivator amplified in breast and ovarian cancer. Science *277*, 965–968.

Beato, M., Herrlich, P., and Schutz, G. (1995). Steroid hormone receptors: many actors in search of a plot. Cell *83*, 851–857.

Berry, M., Metzger, D., and Chambon, P. (1990). Role of the two activating domains of the oestrogen receptor in the cell-type and

promoter-context dependent agonistic activity of the anti-oestrogen 4-hydroxytamoxifen. EMBO J. *9*, 2811–2818.

Bourguet, W., Ruff, M., Chambon, P., Gronemeyer, H., and Moras, D. (1995). Crystal structure of the ligand-binding domain of the human nuclear receptor RXR-α. Nature *375*, 377–382.

Brünger, A.T. (1996). X-PLOR Version 3.843 (New Haven, CT: Yale University).

Brzozowski, A., Pike, A., Dauter, Z., Hubbard, R., Bonn, T., Engstrom, O., Ohman, L., Greene, G., Gustafsson, J., and Carlquist, M. (1997). Molecular basis of agonism and antagonism in the oestrogen receptor. Nature *389*, 753–758.

CCP4. (1994). The CCP4 suite: programs for protein crystallography. Acta Crystallogr. D *50*, 760–763.

Chen, H., Lin, R.J., Schiltz, R.L., Chakravarti, D., Nash, A., Nagy, L., Privalsky, M.L., Nakatani, Y., and Evans, R.M. (1997). Nuclear receptor coactivator ACTR is a novel histone acetyltransferase and forms a multimeric activation complex with P/CAF and CBP/p300. Cell *90*, 569–580.

Danielian, P., White, R., Lees, J., and Parker, M. (1992). Identification of a conserved region required for hormone dependent transcriptional activation by steroid hormone receptors. EMBO J. *11*, 1025–1033.

Ding, S., Anderson, C., Ma, H., Hong, H., Uht, R., Kushner, P., and Stallcup, M. (1998). Nuclear receptor-binding sites of coactivators glucocorticoid receptor interacting protein 1 (GRIP1) and steroid receptor coactivator 1 (SRC-1): multiple motifs with different binding specificities. Mol. Endocrinol. *12*, 302–313.

Esnouf, R.M. (1997). An extensively modified version of MolScript that includes greatly enhanced coloring capabilities. J. Mol. Graph. Model. *15*, 132–134.

Feng, W., Ribeiro, R.C., Wagner, R.L., Nguyen, H., Apriletti, J.W., Fletterick, R.J., Baxter, J.D., Kushner, P.J., and West, B.L. (1998). Hormone-dependent coactivator binding to a hydrophobic cleft on nuclear receptors. Science *280*, 1747–1749.

Furey, W., and Swaminathan, S. (1990). PA33. Am. Cryst. Assoc. Mtg. Abstr. *18*, 73.

Glass, C.K., Rose, D.W., and Rosenfeld, M.G. (1997). Nuclear receptor coactivators. Curr. Opin. Cell Biol. *9*, 222–232.

Gradishar, W.J., and Jordan, V.C. (1997). Clinical potential of new antiestrogens. J. Clin. Oncol. *15*, 840–852.

Grainger, D.J., and Metcalfe, J.C. (1996). Tamoxifen: teaching an old drug new tricks? Nat. Med. *2*, 381–385.

Greene, G., Nolan, C., Engler, J., and Jensen, E. (1980). Monoclonal antibodies to human estrogen receptor. Proc. Natl. Acad. Sci. USA *77*, 5115–5119.

Greene, G., Harris, K., Bova, R., Kinders, R., Moore, B., and Nolan, C. (1988). Purification of T47D human progesterone receptor and immunochemical characterization with monoclonal antibodies. Mol. Endocrinol. *2*, 714–726.

Grese, T.A., Sluka, J.P., Bryant, H.U., Cullinan, G.J., Glasebrook, A.L., Jones, C.D., Matsumoto, K., Palkowitz, A.D., Sato, M., Termine, J.D., et al. (1997). Molecular determinants of tissue selectivity in estrogen receptor modulators. Proc. Natl. Acad. Sci. USA *94*, 14105–14110.

Hanstein, B., Eckner, R., DiRenzo, J., Halachmi, S., Liu, H., Searcy, B., Kurokawa, R., and Brown, M. (1996). p300 is a component of an estrogen receptor coactivator complex. Proc. Natl. Acad. Sci. USA *93*, 11540–11545.

Heery, D., Kalkhoven, E., Hoare, S., and Parker, M. (1997). A signature motif in transcriptional co-activators mediates binding to nuclear receptors. Nature *387*, 733–736.

Hegy, G., Shackleton, C., Carlquist, M., Bonn, T., Engstrom, O., Sjoholm, P., and Witkowska, H. (1996). Carboxymethylation of the human estrogen receptor ligand-binding domain-estradiol complex: HPLC/ESMS peptide mapping shows that cysteine 447 does not react with iodoacetic acid. Steroids *61*, 367–373.

Henttu, P.M., Kalkhoven, E., and Parker, M.G. (1997). AF-2 activity and recruitment of steroid receptor coactivator 1 to the estrogen receptor depend on a lysine residue conserved in nuclear receptors. Mol. Cell. Biol. *17*, 1832–1839.

Hong, H., Kohli, K., Trivedi, A., Johnson, D.L., and Stallcup, M.R. (1996). GRIP1, a novel mouse protein that serves as a transcriptional coactivator in yeast for the hormone binding domains of steroid receptors. Proc. Natl. Acad. Sci. USA *93*, 4948–4952.

Horwitz, K.B., Jackson, T.A., Bain, D.L., Richer, J.K., Takimoto, G.S., and Tung, L. (1996). Nuclear receptor coactivators and corepressors. Mol. Endocrinol. *10*, 1167–1177.

Huang, C.C., Pettersen, E.F., Klein, T.E., Ferrin, T.E., and Langridge, R. (1991). Conic: a fast renderer for space-filling molecules with shadows. J. Mol. Graph. *9*, 230–236, 242.

Jordan, V.C. (1998). Antiestrogenic action of raloxifene and tamoxifen: today and tomorrow. J. Natl. Cancer Inst. *90*, 967–971.

Jordan, V.C., and Gosden, B. (1982). Importance of the alkylaminoethoxy side-chain for the estrogenic and antiestrogenic actions of tamoxifen and trioxifene in the immature rat uterus. Mol. Cell. Endocrinol. *27*, 291–306.

Kamei, Y., Xu, L., Heinzel, T., Torchia, J., Kurokawa, R., Gloss, B., Lin, S.C., Heyman, R.A., Rose, D.W., Glass, C.K., and Rosenfeld, M.G. (1996). A CBP integrator complex mediates transcriptional activation and AP-1 inhibition by nuclear receptors. Cell *85*, 403–414.

Kato, S., Endoh, H., Masuhiro, Y., Kitamoto, T., Uchiyama, S., Sasaki, H., Masushige, S., Gotoh, Y., Nishida, E., Kawashima, H., et al. (1995). Activation of the estrogen receptor through phosphorylation by mitogen-actived protein kinase. Science *270*, 1491–1494.

Kleywegt, G.J., and Jones, T.A. (1994). Halloween...masks and bones. In From First Map to Final Model, S. Bailey, R. Hubbard, and D. Waller, eds. (Warrington, England: SERC Daresbury Laboratory).

Korach, K. (1994). Insights from the study of animals lacking functional estrogen receptor. Science *266*, 1524–1527.

Kuiper, G.G., Carlsson, B., Grandien, K., Enmark, E., Haggblad, J., Nilsson, S., and Gustafsson, J.A. (1997). Comparison of the ligand binding specificity and transcript tissue distribution of estrogen receptors alpha and beta. Endocrinology *138*, 863–870.

Kumar, V., Green, S., Stack, G., Berry, M., Jin, J.-R., and Chambon, P. (1987). Functional domains of the human estrogen receptor. Cell *51*, 941–951.

Le Douarin, B., Nielsen, A.L., Garnier, J.M., Ichinose, H., Jeanmougin, F., Losson, R., and Chambon, P. (1996). A possible involvement of TIF1 alpha and TIF1 beta in the epigenetic control of transcription by nuclear receptors. EMBO J. *15*, 6701–6715.

Li, H., Gomes, P.J., and Chen, J.D. (1997). RAC3, a steroid/nuclear receptor-associated coactivator that is related to SRC-1 and TIF2. Proc. Natl. Acad. Sci. USA *94*, 8479–8484.

Merritt, E.A., and Anderson, W.F. (1994). Raster3D Version 2.0: a program for photorealistic molecular structures. Acta Crystallogr. D *50*, 219–220.

Moras, D., and Gronemeyer, H. (1998). The nuclear receptor ligand-binding domain: structure and function. Curr. Opin. Cell Biol. *10*, 384–391.

Muller, K., Amman, H.J., Doran, D.M., Gerber, P.R., Gubernator, K., and Schrepfer, G. (1988). MOLOC: A molecular modeling program. Bull. Soc. Chim. Belg. *97*, 655–667.

Murshudov, G.N., Vagin, A.A., and Dodson, E.J. (1997). Refinement of macromolecular structures by the maximum-likelihood method. Acta Crystallogr. D *53*, 240–255.

Nicholls, A., Sharp, K., and Honig, B. (1991). Protein folding and association: insights from the interfacial and thermodynamic properties of hydrocarbons. Proteins *11*, 281–296.

Norris, J.D., Fan, D., Stallcup, M.R., and McDonnell, D.P. (1998). Enhancement of estrogen receptor transcriptional activity by the coactivator GRIP-1 highlights the role of activation function 2 in determining estrogen receptor pharmacology. J. Biol. Chem. *273*, 6679–6688.

Onate, S.A., Tsai, S.Y., Tsai, M.-J., and O'Malley, B.W. (1995). Sequence and characterization of a coactivator for the steroid hormone receptor family. Science *270*, 1354–1357.

Otwinowski, Z., and Minor, W. (1997). Processing of x-ray diffraction data collected in oscillation mode. Methods Enzymol. *276*, 307–326.

Renaud, J., Rochel, N., Ruff, M., Vivat, V., Chambon, P., Gronemeyer,

H., and Moras, D. (1995). Crystal structure of the RAR-γ ligand-binding domain bound to all-trans retinoic acid. Nature *378*, 681–689.

Robertson, D.W., Katzenellenbogen, J.A., Hayes, J.R., and Katzenellenbogen, B.S. (1982). Antiestrogen basicity—activity relationships: a comparison of the estrogen receptor binding and antiuterotrophic potencies of several analogues of (Z)-1,2-diphenyl-1-[4-[2-(dimethylamino)ethoxy]phenyl]-1- butene (tamoxifen, Nolvadex) having altered basicity. J. Med. Chem. *25*, 167–171.

Seielstad, D., Carlson, K., Katzenellenbogen, J., Kushner, P., and Greene, G. (1995). Molecular characterization by mass spectrometry of the human estrogen receptor ligand-binding domain expressed in *Escherichia coli*. Mol. Endocrinol. *9*, 647–658.

Smigel, K. (1998). Breast cancer prevention trial shows major benefit, some risk. J. Natl. Cancer Inst. *90*, 647–648.

Smith, E., Boyd, J., Frank, G., Takahashi, H., Cohen, R., Specker, B., Williams, T., Lubahn, D., and Korach, K. (1994). Estrogen resistance caused by a mutation in the estrogen-receptor gene in a man. N. Engl. J. Med. *331*, 1056–1061.

Tanenbaum, D.M., Wang, Y., Williams, S.P., and Sigler, P.B. (1998). Crystallographic comparison of the estrogen and progesterone receptor's ligand binding domains. Proc. Natl. Acad. Sci. USA *95*, 5998–6003.

Tora, L., Mullick, A., Metzger, D., Ponglikitmongkol, M., Park, I., and Chambon, P. (1989). The cloned human oestrogen receptor contains a mutation which alters its hormone binding properties. EMBO J. *8*, 1981–1986.

Torchia, J., Rose, D., Inostroza, J., Kamel, Y., Westin, S., Glass, C., and Rosenfeld, M. (1997). The transcriptional co-activator p/CIP binds CBP and mediates nuclear-receptor function. Nature *387*, 677–684.

Tsai, M.J., and O'Malley, B.W. (1994). Molecular mechanisms of action of steroid/thyroid receptor superfamily members. Annu. Rev. Biochem. *63*, 451–486.

Voegel, J.J., Heine, M.J.S., Zechel, C., Chambon, P., and Gronemeyer, H. (1996). TIF2, a 160 kDa transcriptional mediator for the ligand-dependent activation function AF-2 of nuclear receptors. EMBO J. *15*, 3667–3675.

Voegel, J.J., Heine, M.J., Tini, M., Vivat, V., Chambon, P., and Gronemeyer, H. (1998). The coactivator TIF2 contains three nuclear receptor-binding motifs and mediates transactivation through CBP binding-dependent and -independent pathways. EMBO J. *17*, 507–519.

Wallace, A.C., Laskowski, R.A., and Thornton, J.M. (1995). LIGPLOT: a program to generate schematic diagrams of protein-ligand interactions. Protein Eng. *8*, 127–134.

Wrenn, C., and Katzenellenbogen, B. (1993). Structure-function analysis of the hormone binding domain of the human estrogen receptor by region-specific mutagenesis and phenotypic screening in yeast. J. Biol. Chem. *268*, 24089–24098.

Wurtz, J.M., Bourguet, W., Renaud, J.P., Vivat, V., Chambon, P., Moras, D., and Gronemeyer, H. (1996). A canonical structure for the ligand-binding domain of nuclear receptors. Nat. Struct. Biol. *3*, 87–94.

**Brookhaven Protein Data Bank Accession Numbers**

Coordinates have been deposited with the PDB for the DES-ERα LBD-GRIP1 NR box II peptide complex (2ERD) and for the OHT-ERα LBD complex (2ERT).

**Note Added in Proof**

During the course of this work, we received a draft of a manuscript (Darimont, B.D., et al. [1998]. Structure and specificity of nuclear receptor-coactivator interactions. Genes Dev. *12*, 3343–3356) describing structural studies of the complex between TRβ and the GRIP1 NR box II peptide and biochemical studies of GRIP1 binding to TRβ and GR. We have included references to this work in the text as Darimont et al. (1998). The general features of the TRβ/GRIP1 NR box II peptide complex and the recently described PPARγ/SRC-1 peptide complex (Nolte, R.T., et al. [1998]. Ligand binding and co-activator assembly of the peroxisome proliferator-activated receptor-γ. Nature *395*, 137–143) are very similar to those of the ERα/GRIP1 NR box II peptide complex discussed here, suggesting that the mechanisms of NR box recognition are conserved across NRs.